Structural stability of the Wadsley-type bronzes β-$Ag_{0.33}V_2O_5$ and β-$Li_{0.33}V_2O_5$ on compression: A breakdown of the two-leg ladder system in the nonsuperconducting high-pressure phase of β-$Li_{0.33}V_2O_5$

A. Grzechnik,[1,*] Y. Ueda,[2,3] T. Yamauchi,[2] M. Hanfland,[4] P. Hering,[5] V. Potapkin,[5] and K. Friese[5]

[1]*Institute of Crystallography, RWTH Aachen University, 52060 Aachen, Germany*

[2]*Institute for Solid State Physics, University of Tokyo, Kashiwa, Chiba 277-8581, Japan*

[3]*Toyota Chemical and Physical Research Institute, Nagakute, Aichi 480-1192, Japan*

[4]*European Synchrotron Radiation Facility, BP 220, 38043 Grenoble, France*

[5]*Jülich Centre for Neutron Science-2, Research Centre Jülich GmbH, 52425 Jülich, Germany*

(Received 25 February 2015; revised manuscript received 11 May 2015; published 27 May 2015)

Structural stabilities of the Wadsley-type bronzes β-$Ag_{0.33}V_2O_5$ and β-$Li_{0.33}V_2O_5$ (both C2/m, $Z = 6$) have been studied with single-crystal x-ray diffraction in diamond anvil cells at room temperature to 8 and 13 GPa, respectively. β-$Ag_{0.33}V_2O_5$ is stable at least to 8 GPa. β-$Li_{0.33}V_2O_5$ undergoes two phase transitions at about 9 and 11 GPa due to relative displacements of the adjacent octahedral vanadate layers. In the intermediate phase between 9 and 11 GPa, very strong one-dimensional diffuse scattering is observed, indicating the presence of stacking faults. The structural refinements (C2/m, $Z = 6$) of the data above 11 GPa reveal that the layers of VO_6 octahedra remain essentially intact. However, the relative position of the chains of edge-sharing VO_5 tetragonal pyramids with respect to the octahedral layers is changed. As a result, the tunnels populated by the Li^1+ cations collapse on compression. The distribution of the Li^1+ cations in the vanadate framework is fully ordered in the polymorph above 11 GPa. The present structural data could be used to better understand the pressure-induced superconductivity in all the Wadsley-type bronzes β-$A_{0.33}V_2O_5$ (A = Li, Na, Ag).

DOI: 10.1103/PhysRevB.91.174113 PACS number(s): 61.05.cp, 61.50.Ks, 61.66.Fn

I. INTRODUCTION

β-$A_{0.33}V_2O_5$ bronzes (A = Li, Na, Ag) have a crystal structure (C2/m, Z = 6) [1] (Fig. 1) built of zigzag double strings of distorted VO_6 octahedra that form layers in the (a,b) plane by joining corners. The adjacent layers are linked by chains of edge-sharing VO_5 tetragonal pyramids resulting in tunnels along the b axis. Each tunnel is partially occupied by the A^+ cations.

At low temperatures and atmospheric pressure, these bronzes undergo metal-insulator (MI) phase transitions resulting from charge ordering of mixed-valence vanadium [2–4]. The phase transition in β-$Li_{0.33}V_2O_5$ at 170 K is supposedly associated with a formation of the $2a \times 2b \times c$ superstructure [2]. β-$Na_{0.33}V_2O_5$ transforms first to the $a \times 2b \times c$ superstructure (space group $P2_1/a$) at 260 K and then to the $a \times 6b \times c$ superstructure (space group $P2_1/a$) at the MI transition ($T_{MI} \approx 130$ K) [3]. It was suggested that the MI transition in $Na_{0.33}V_2O_5$ is not of a simple order-disorder type but rather charge-density-wave like [4].

The low-dimensional β-$A_{0.33}V_2O_5$ bronzes are superconducting under high pressure below approximately 9 K [5–9]. The superconductivity occurs at about 7 GPa in β-$Na_{0.33}V_2O_5$ and β-$Ag_{0.33}V_2O_5$ and at about 9 GPa in β-$Li_{0.33}V_2O_5$. The mechanism of the superconductivity in these bronzes has not been presented so far. One of the most fundamental issues to be resolved is the determination of the underlying crystal structures. Resistivity measurements as a function of pressure at room temperature demonstrated that β-$Li_{0.33}V_2O_5$ undergoes a reversible phase transition to a nonsuperconducting polymorph above 10 GPa [8]. It has been suggested [8] that the structure of this phase is of key importance for the understanding of the mechanism of superconductivity in all the vanadium bronzes.

In this study, we are interested in β-$Li_{0.33}V_2O_5$ and β-$Ag_{0.33}V_2O_5$ studied with single-crystal x-ray diffraction in diamond anvil cells at room temperature. Our aim is to investigate their high-pressure behaviors and crystal structures in relation to those occurring at low temperatures in β-$A_{0.33}V_2O_5$ [2,3] as well as to clarify the pressure-induced anomalies in resistivity observed in β-$Li_{0.33}V_2O_5$ at high pressures and room temperature [8].

II. EXPERIMENTAL PROCEDURE

The crystals of β-$Li_{0.33}V_2O_5$ and β-$Ag_{0.33}V_2O_5$ studied here are from the same batches as those previously used to determine physical properties of the two materials at various pressure and temperature conditions [2,6,8].

Ruby luminescence method [10] was used for pressure calibration during all our experiments.

The single crystals of both materials were investigated in diamond anvil cells of the Ahsbahs type [11] to about 9 GPa at room temperature using a STOE IPDS-II (Mo-Kα) diffractometer. The 1:4 mixture of ethanol–methanol was used as a hydrostatic pressure medium. All data sets were indexed and integrated with the STOE software X-Area [12]. The collected intensities were too few and too weak so that apart from lattice parameters it was not possible to determine and refine crystal structures.

β-$Li_{0.33}V_2O_5$ was subsequently studied using single-crystal diffraction upon compression in a membrane driven diamond anvil cell modified for Boehler-Almax anvils at room temperature on the ID09a beamline ($\lambda = 0.414\,601$ Å, a Mar555

*grzechnik@xtal.rwth-aachen.de

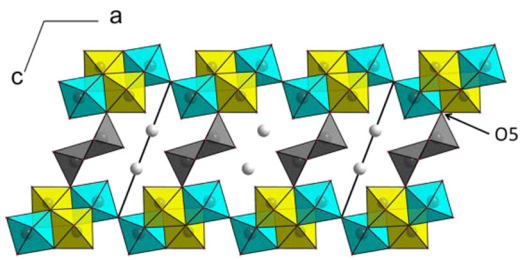

FIG. 1. (Color online) Crystal structure of β-$Li_{0.33}V_2O_5$ at atmospheric pressure (C2/m, $Z = 6$). The polyhedra around the V1, V2, and V3 atoms are drawn yellow, cyan, and dark gray, respectively. The gray symbols are the Li atoms. The O5 oxygen atom is indicated.

flat panel detector) at the European Synchrotron Radiation Facility (Grenoble, France) [13]. Helium was used as a hydrostatic pressure medium. All data sets were collected in one cycle in which the crystal was always at hydrostatic pressure conditions.

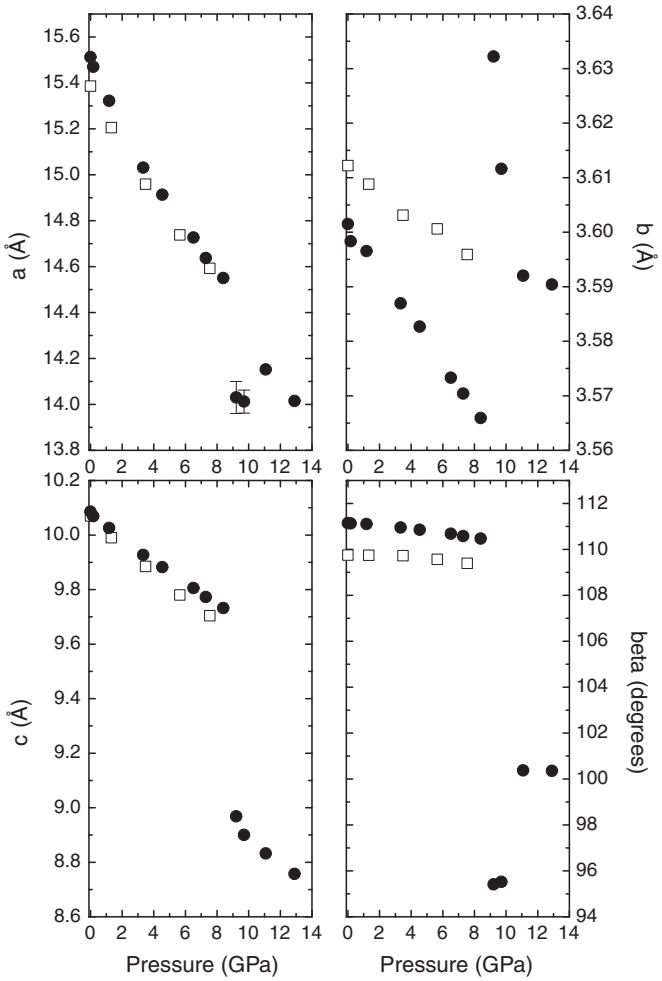

FIG. 2. Pressure dependence of lattice parameters in β-$Li_{0.33}V_2O_5$ (full symbols, synchrotron data) and β-$Ag_{0.33}V_2O_5$ (open symbols, laboratory x-ray data). The estimated standard deviations are shown when larger than the symbols.

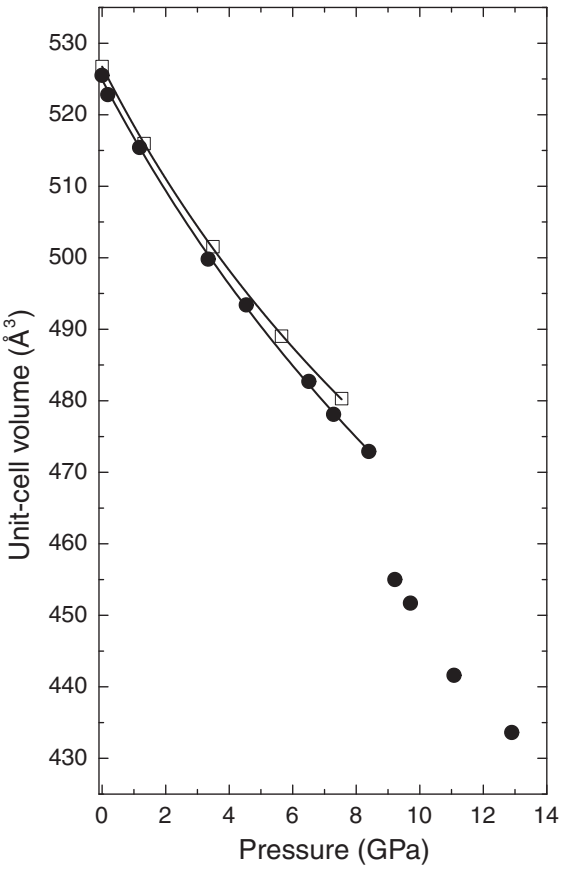

FIG. 3. Pressure dependence of unit-cell volumes in β-$Li_{0.33}V_2O_5$ (full symbols, synchrotron data) and β-$Ag_{0.33}V_2O_5$ (open symbols, laboratory data). The estimated standard deviations are smaller than the symbols. The solid lines are the equation-of-state fits to the compressibility data.

All data were indexed and integrated with the Crysalis software [14]. The structural model for the ambient-pressure data was taken from Ref. [1]. For each data set upon compression to 8.40 GPa, the model resulting from the next lowest pressure point was used as an input for the structural refinement.

All reflections in the diffraction pattern at 11.08 GPa could be indexed with a monoclinic cell. The observed extinction rules indicated a C-centered lattice. As the internal R values for the point group symmetries 2, m and 2/m were comparable, the space group C2/m was used to solve the structure for this pressure point. The structure solution was carried out with the program SIR97 [15] using direct methods and yielded all vanadium atom positions as well as part of the oxygen atoms. The remaining atoms were found from the difference Fourier maps. Trial refinements using the noncentrosymmetric monoclinic space groups C2 and Cm did not lead to a better quality of the fit to the data and were therefore discarded. The final refined model in C2/m was subsequently an input for the data set at 12.87 GPa.

Each structural model was refined with the program Jana2006 [16] using the methodology described in reference

TABLE I. Experimental data for the single-crystal measurements on β-$Li_{0.33}V_2O_5$ (C2/m, $Z = 6$) up to about 9 GPa.

Pressure (GPa)	0.0001	0.18	1.78	3.34	4.58	6.51	7.29	8.40
Crystal data								
a (Å)	15.51 (1)	15.47(1)	15.32(1)	15.03(1)	14.91(1)	14.73(1)	14.64(1)	14.55(1)
b (Å)	3.6015(1)	3.5983(2)	3.5965(2)	3.5869(2)	3.5827(1)	3.5733(1)	3.5704(1)	3.5659(2)
c (Å)	10.0855(13)	10.0688(14)	10.0256(16)	9.9270(15)	9.8820(14)	9.8056(13)	9.7723(13)	9.7320(14)
β (°)	111.14(4)	111.13(4)	111.10(5)	110.95(4)	110.85(4)	110.68(4)	110.58(4)	110.47(4)
V (Å^3)	525.5	522.8	515.4	499.8	493.4	482.7	478.1	473.0
ρ(g cm^{-3})	3.491	3.509	3.559	3.670	3.718	3.800	3.837	3.878
μ(mm^{-1})	1.095	1.100	1.116	1.151	1.166	1.192	1.203	1.216
Data collection								
No. meas. refl.	489	490	486	466	441	449	453	442
Range of hkl	$-9 \leqslant h \leqslant 10$	$-9 \leqslant h \leqslant 9$	$-9 \leqslant h \leqslant 9$	$-9 \leqslant h \leqslant 9$	$-8 \leqslant h \leqslant 9$	$-8 \leqslant h \leqslant 9$	$-8 \leqslant h \leqslant 9$	$-8 \leqslant h \leqslant 8$
	$-5 \leqslant k \leqslant 5$	$-4 \leqslant k \leqslant 4$	$-4 \leqslant k \leqslant 4$	$-4 \leqslant k \leqslant 4$	$-4 \leqslant k \leqslant 4$	$-4 \leqslant k \leqslant 4$	$-4 \leqslant k \leqslant 4$	$-4 \leqslant k \leqslant 4$
	$-14 \leqslant l \leqslant 15$	$-11 \leqslant l \leqslant 12$	$-12 \leqslant l \leqslant 11$	$-11 \leqslant l \leqslant 12$	$-11 \leqslant l \leqslant 12$	$-11 \leqslant l \leqslant 11$	$-12 \leqslant l \leqslant 12$	$-11 \leqslant l \leqslant 11$
No. obs.refl.[a]	245	207	204	197	182	192	178	181
$R(\text{int})_{\text{obs}}$[b]	1.20	1.78	1.99	1.57	3.95	2.05	1.42	1.17
Refinement								
R_{obs}	4.55	4.12	4.29	3.76	4.90	3.56	3.82	3.23
wR_{obs}	5.54	5.30	5.47	5.00	5.69	4.98	4.92	4.44
GoF$_{\text{obs}}$	3.73	3.68	3.70	3.65	3.58	3.53	3.93	3.57
No. pars.	45	45	45	45	45	45	45	45

[a]Criterion for the observed reflections is $|F_{\text{obs}}| > 3\sigma$.

[b]All agreement factors are given in %, weighing scheme is $1/[\sigma^2(F_{\text{obs}}) + (0.01F_{\text{obs}})^2]$.

[17–19]. All the trials to determine the strongly polytypic structure in the pressure range 9.2–11.0 GPa failed.

III. RESULTS AND DISCUSSION

Upon compression, the crystal structure of β-$Ag_{0.33}V_2O_5$ is stable at least to about 8 GPa, i.e., to the highest pressure at which it was possible to collect diffracted intensities using laboratory equipment. Lattice parameters and unit-cell volumes of this material in Figs. 2 and 3, respectively, are shown as the open symbols.

The analysis of the synchrotron data for β-$Li_{0.33}V_2O_5$ revealed that this material undergoes a two-phase transition at 9 GPa and 11 GPa, associated with discontinuities in the pressure dependence of the lattice parameters and unit-cell volumes (the full symbols in Figs. 2 and 3). At all pressures, the data could be indexed with the C-centered monoclinic lattice ($Z = 6$). The b lattice parameter is the least compressible in the low-pressure phase and it increases during the first-phase transition at 9.2 GPa. Our present findings confirm the previous observation that β-$Li_{0.33}V_2O_5$ becomes structurally unstable around 10 GPa as seen in the resistivity curves upon compression at room temperature [8]. We do not find any reflections in all our high-pressure data that would evidence the formation of the superstructures previously reported for β-$Li_{0.33}V_2O_5$ [2] and β-$Na_{0.33}V_2O_5$ [3] at low temperatures and atmospheric pressure. The phase transitions in β-$Li_{0.33}V_2O_5$ are reversible [8].

The axial, angular, and bulk compressibilities of β-$Ag_{0.33}V_2O_5$ and β-$Li_{0.33}V_2O_5$ to about 9 GPa are very similar (Figs. 2 and 3). The P-V data for the low-pressure phases of the two materials could be fitted with the third-order Birch-Murnaghan equations of state–β-$Li_{0.33}V_2O_5$: $V_0 = 524.9(5)$ Å^3, $B_0 = 62(3)$ GPa, $B' = 5.1(8)$; β-$Ag_{0.33}V_2O_5$: $V_0 = 526.8(4)$ Å^3, $B_0 = 60(2)$ GPa, $B' = 6.9(8)$. The reported bulk modulus for β-$Na_{0.33}V_2O_5$ is slightly lower, $B_0 = 53.8(1.5)$ GPa [20].

The details of the refined structural models for β-$Li_{0.33}V_2O_5$ to 8.40 GPa are shown in Tables I and II. The V1 and V2 atoms are six-fold coordinated by oxygen. They are displaced from the centers of the octahedra so that the V-O bonds vary between 1.59 and 2.4 Å at ambient pressure (Fig. 4). The V3 atom has five oxygen bonds of similar length (1.6–2.0 Å). The sixth V3-O bond is considerably longer (2.61 Å), so that the coordination around V3 is better described as distorted tetragonal pyramid (Fig. 1). As can be seen from Fig. 4, all the V-O bond distances up to 8.40 GPa decrease only slightly. More sensitive to increasing pressure are the O-O distances across the channels (Figs. 1, 5, and 6). In particular, the O8-O8 distance decreases by nearly 20% upon compression to about 8.4 GPa (Figs. 5 and 6), indicating the pressure-induced closure of the channel running along the b axis.

An inspection of the reconstructed reciprocal space (Fig. 7) clearly shows that a very strong one-dimensional diffuse scattering along c^* is observed in the intermediate phase of $Li_{0.33}V_2O_5$ between 9.2 and 11 GPa. The data at 9.22 GPa could be indexed with the lattice parameters $a = 14.03(7)$ Å, $b = 3.6322(13)$, $c = 8.968(3)$ Å, and $\beta = 95.41(9)°$. The observed extinction rules are in accordance with a monoclinic C-centered lattice. Despite several attempts to solve the structure of the intermediate polymorph, it was not possible to obtain a reasonable model of this phase.

The diffuse scattering disappears above 11 GPa (Fig. 7) and at these higher pressures a structure solution and refinement

TABLE II. Refined structural parameters in β-$Li_{0.33}V_2O_5$ to about 9 GPa. The occupancies of the sites for the V and O atoms are all equal to 1. The occupancies of the sites for the Li atoms are all equal to 0.5.

	x	y	z	U_{iso}
Ambient				
V1	0.3398(3)	0	0.106 42(18)	0.015(3)
V2	0.1182(3)	0	0.116 76(19)	0.018(4)
V3	0.2899(4)	0	0.4140(2)	0.008(4)
O1	0	0	0	0.0156(19)
O2	0.8166(13)	0	0.0575(7)	0.0119(12)
O3	0.6344(13)	0	0.0742(7)	0.0096(12)
O4	0.4397(18)	0	0.2264(11)	0.037(2)
O5	0.2667(13)	0	0.2258(7)	0.0097(12)
O6	0.1117(14)	0	0.2721(8)	0.0130(13)
O7	0.2443(13)	0	0.5740(7)	0.0100(12)
O8	0.4042(19)	0	0.4848(12)	0.029(2)
Li	0.002(11)	0	0.360(6)	0.046(12)
0.18 GPa				
V1	0.3398(3)	0	0.106 16(19)	0.016(4)
V2	0.1177(4)	0	0.1167(2)	0.028(5)
V3	0.2902(4)	0	0.4141(3)	0.010(4)
O1	0	0	0	0.0095(19)
O2	0.8139(14)	0	0.0563(8)	0.0110(13)
O3	0.6363(13)	0	0.0756(7)	0.0089(12)
O4	0.441(2)	0	0.2268(11)	0.039(2)
O5	0.2686(14)	0	0.2274(8)	0.0081(13)
O6	0.1102(16)	0	0.2718(9)	0.0135(14)
O7	0.2450(14)	0	0.5738(8)	0.0091(12)
O8	0.401(2)	0	0.4844(13)	0.031(3)
Li	0.007(11)	0	0.356(6)	0.042(11)
1.78 GPa				
V1	0.3410(3)	0	0.106 06(19)	0.018(4)
V2	0.1174(4)	0	0.1184(2)	0.026(5)
V3	0.2912(5)	0	0.4151(3)	0.006(4)
O1	0	0	0	0.009(2)
O2	0.8153(15)	0	0.0564(9)	0.0101(14)
O3	0.6348(13)	0	0.0765(8)	0.0071(13)
O4	0.445(2)	0	0.2277(12)	0.037(3)
O5	0.2679(15)	0	0.2267(8)	0.0058(13)
O6	0.1067(17)	0	0.2727(9)	0.0111(14)
O7	0.2459(14)	0	0.5744(8)	0.0077(13)
O8	0.407(2)	0	0.4868(13)	0.028(2)
Li	−0.010(11)	0	0.358(6)	0.043(12)
3.34 GPa				
V1	0.3421(3)	0	0.105 01(18)	0.016(4)
V2	0.1187(4)	0	0.1222(2)	0.022(4)
V3	0.2929(5)	0	0.4168(3)	0.008(4)
O1	0	0	0	0.0090(19)
O2	0.8158(15)	0	0.0561(8)	0.0081(13)
O3	0.6369(13)	0	0.0815(7)	0.0076(12)
O4	0.447(2)	0	0.2265(11)	0.032(2)
O5	0.2696(15)	0	0.2276(8)	0.0069(13)
O6	0.1087(16)	0	0.2784(8)	0.0116(14)
O7	0.2436(14)	0	0.5742(8)	0.0080(13)
O8	0.408(2)	0	0.4870(13)	0.026(2)
Li	0.007(12)	0	0.366(6)	0.042(12)

TABLE II. (*Continued*.)

	x	y	z	U_{iso}
4.58 GPa				
V1	0.3437(5)	0	0.1047(2)	0.011(5)
V2	0.1207(5)	0	0.1248(3)	0.012(6)
V3	0.2940(6)	0	0.4179(3)	0.0093(7)
O1	0	0	0	0.014(3)
O2	0.816(2)	0	0.0566(11)	0.0092(16)
O3	0.6371(17)	0	0.0827(10)	0.0082(16)
O4	0.444(3)	0	0.2255(15)	0.034(3)
O5	0.271(2)	0	0.2269(12)	0.0076(16)
O6	0.112(2)	0	0.2814(11)	0.0109(17)
O7	0.2452(18)	0	0.5757(10)	0.0054(14)
O8	0.409(3)	0	0.4881(17)	0.027(3)
Li	−0.016(13)	0	0.361(7)	0.033(12)
6.51 GPa				
V1	0.3436(3)	0	0.103 81(18)	0.018(4)
V2	0.1196(4)	0	0.1264(2)	0.024(5)
V3	0.2946(4)	0	0.4187(2)	0.010(4)
O1	0	0	0	0.009(2)
O2	0.8183(16)	0	0.0562(9)	0.0076(12)
O3	0.6376(13)	0	0.0849(7)	0.0057(12)
O4	0.449(2)	0	0.2257(11)	0.028(2)
O5	0.2714(17)	0	0.2280(9)	0.0051(13)
O6	0.1072(17)	0	0.2831(8)	0.0090(14)
O7	0.2444(14)	0	0.5761(8)	0.0064(12)
O8	0.415(2)	0	0.4896(14)	0.026(2)
Li	0.009(13)	0	0.372(7)	0.041(11)
7.29 GPa				
V1	0.3446(4)	0	0.103 78(18)	0.015(4)
V2	0.1198(4)	0	0.1275(2)	0.021(5)
V3	0.2949(5)	0	0.4192(2)	0.012(5)
O1	0	0	0	0.012(2)
O2	0.8198(17)	0	0.0570(9)	0.0103(13)
O3	0.6379(14)	0	0.0868(8)	0.0091(13)
O4	0.449(2)	0	0.2254(11)	0.029(2)
O5	0.2701(18)	0	0.2270(9)	0.0086(13)
O6	0.1093(19)	0	0.2850(9)	0.0122(14)
O7	0.2443(14)	0	0.5770(8)	0.0086(12)
O8	0.415(2)	0	0.4894(14)	0.029(2)
Li	0.007(12)	0	0.370(6)	0.034(9)
8.40 GPa				
V1	0.3451(3)	0	0.103 44(16)	0.017(4)
V2	0.1199(3)	0	0.12883(19)	0.020(4)
V3	0.2958(4)	0	0.4199(2)	0.012(4)
O1	0	0	0	0.0094(19)
O2	0.8185(14)	0	0.0555(8)	0.0082(11)
O3	0.6379(13)	0	0.0877(7)	0.0067(11)
O4	0.4520(19)	0	0.2259(10)	0.0254(17)
O5	0.2707(16)	0	0.2270(8)	0.0072(12)
O6	0.1096(16)	0	0.2873(8)	0.0094(13)
O7	0.2455(14)	0	0.5781(7)	0.0078(11)
O8	0.414(2)	0	0.4895(13)	0.028(2)
Li	0.000(11)	0	0.371(6)	0.036(9)

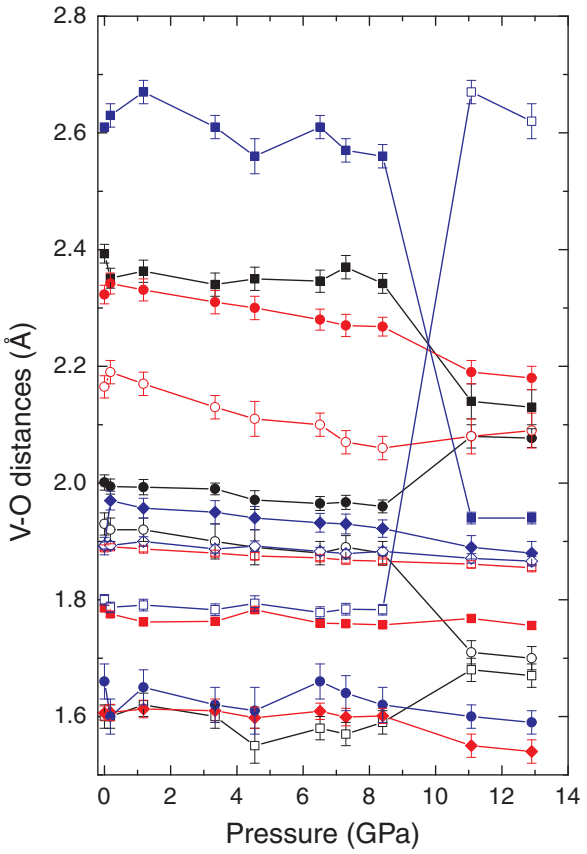

FIG. 4. (Color online) Pressure dependence of the V-O distances in the VO_6 and VO_5 polyhedra in β-$Li_{0.33}V_2O_5$.The lines are guides for the eye. The symbols in black, red, and blue are for the V1-O, V2-O, and V3-O distances, respectively.

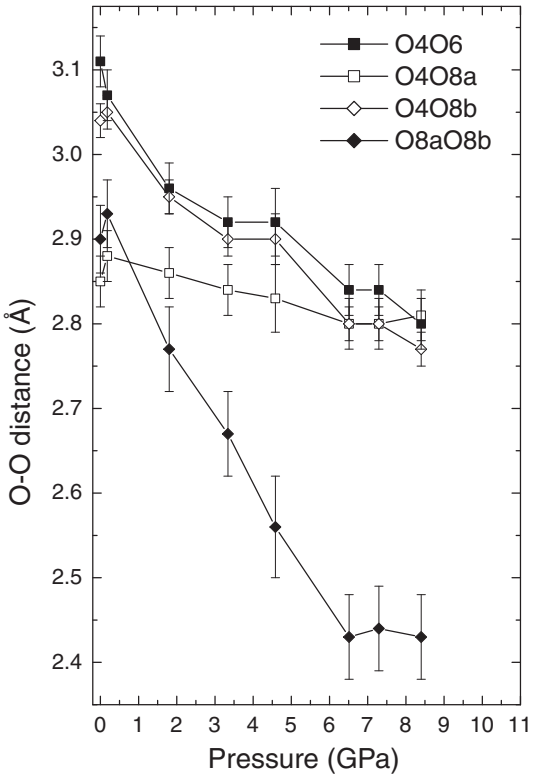

FIG. 6. Pressure dependence of selected O-O distances across the channels in the low-pressure structure of β-$Li_{0.33}V_2O_5$ (see Fig. 5 for the legend explaining the labels of the O atoms). The lines are guides for the eye.

were successful (Tables III and IV). The structure of the new polymorph above 11GPa is shown in Fig. 8. As can be seen from a comparison of the ambient- and high-pressure structures (Figs. 1 and 8), the octahedral layers formed around the V1 and V2 atoms stay essentially identical. It is their relative orientation from one layer to the neighboring one that is different in both polymorphs. The stacking of the octahedral layers in the high-pressure phase can be obtained from the one in the low-pressure polymorph by applying a relative shift of $\Delta x \approx ¼$ to a neighboring layer.

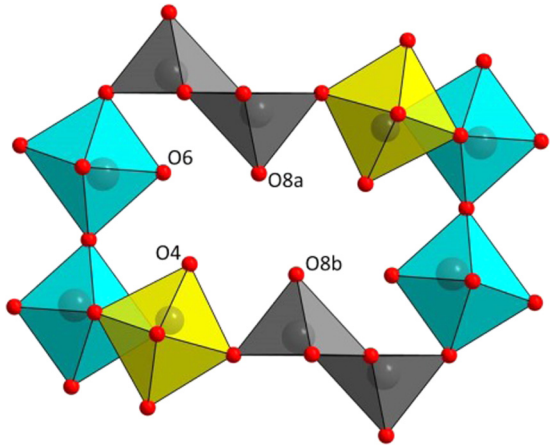

FIG. 5. (Color online) A fragment of the low-pressure structure of β-$Li_{0.33}V_2O_5$ showing the channel along the b axis with some of the O sites labeled. The polyhedra around the V1, V2, and V3 atoms are drawn yellow, cyan, and dark gray, respectively.

The connection of the octahedral layers via the double pyramids around V3 is also significantly changed. In the ambient-pressure structure, the chains of tetragonal pyramids are connected to the octahedral layers through the oxygen atom O5, which belongs to the common edge of the octahedra around V1 and V2 (Fig. 1). In the high-pressure structure the oxygen atom O4, which connects the tetragonal pyramids with the octahedral layers, is exclusively connected to the octahedra around V1 (Fig. 8).

Apart from the five nearest-neighbor oxygen atoms which form the tetragonal pyramid around V3, there is also one significantly longer bond (V3-O > 2.5 Å) with an additional oxygen (Fig. 4). In the low-pressure polymorph this long distance is formed with the oxygen atom O6. In the high-pressure polymorph this distance is drastically shortened to below 2 Å as a consequence of the relative shift of the octahedral layers. At the same time, the V3-O5 distance, which is well below 2 Å in the low-pressure structure, is significantly increased to above 2.6 Å in the high-pressure structure (Fig. 4). This implies that the overall shape of the coordination polyhedra around V3 in both structures is very similar, although the additional longer

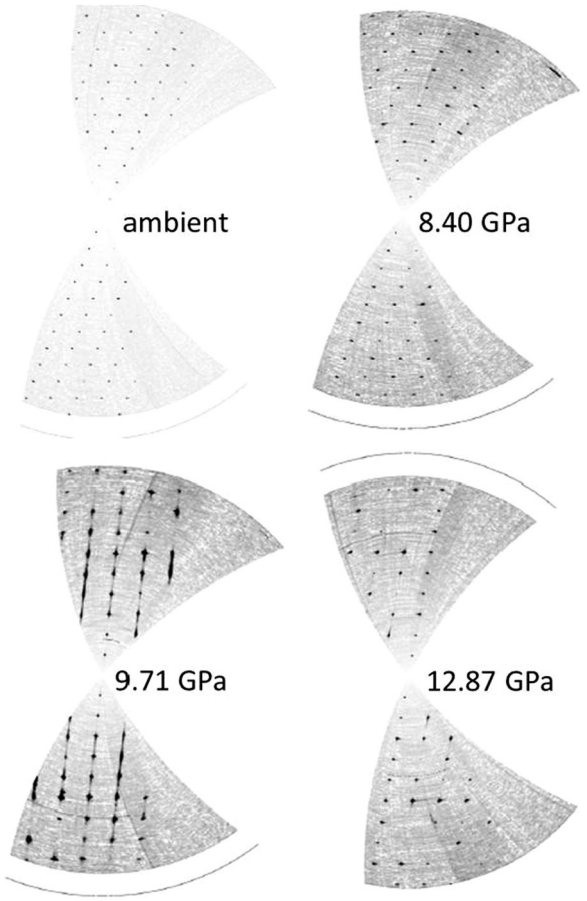

FIG. 7. Reconstructions of the reciprocal space in β-$Li_{0.33}V_2O_5$ at various pressures in the (*h0l*) projection. The reconstructions for the data below 9 GPa correspond to the ambient-pressure structure. The reconstruction for the data at 9.71 GPa corresponds to the intermediate phase in which strong one-dimensional diffuse scattering along c^* is observed. The reconstruction for the data at 12.87 GPa corresponds to the new polymorph whose crystal structure is discussed in this work. The angles β^* between a^* (a horizontal direction) and c^* at pressures below 9 GPa, at 9.71 GPa, and at 12.87 GPa are about 70°, 85°, and 80°, respectively.

bond to the next-nearest oxygen atom is formed with different atoms. These observations clearly show that in contrast to other vanadates [21,22] there is no pressure-induced increase of the coordination numbers of vanadium in $Li_{0.33}V_2O_5$. We also find no evidence in our data for the charge ordering of mixed-valence vanadium at all pressures reached in this study.

Another major change in the structure concerns the distribution of the Li^{1+} ions. In the low-pressure polymorph, Li is located at the Wyckoff position *4i* (*x, 0, z*) on the mirror plane perpendicular to the *b* axis with the *x* coordinate close to 0 and the *z* coordinate, depending on the pressure, between 0.36 and 0.375 (Table II). According to the chemical composition, only two Li^{1+} cations are accommodated in one unit cell, so that the four symmetry equivalent sites for Li are only half occupied. Consequently, a certain degree of disorder is implied. In the high-pressure structure, the Li^{1+} cation is at the Wyckoff special position *2c* (*0, 0, 0.5*). This implies a higher-symmetry site (2/m). Therefore, there are only two

TABLE III. Experimental data for the single-crystal measurements on β-$Li_{0.33}V_2O_5$ (C2/m, $Z = 6$) at 11.08 and 12.87 GPa.

Pressure (GPa)	11.08	12.87
Crystal data		
a (Å)	14.152(3)	14.015(3)
b (Å)	3.5920(1)	3.5904(1)
c (Å)	8.8322(5)	8.7570(5)
β (°)	100.37(1)	100.35(1)
V (Å^3)	441.6	433.6
ρ(g cm^{-3})	4.154	4.232
μ(mm^{-1})	1.302	1.327
Data collection		
No. meas. refl.	385	376
Range of *hkl*	$-9 \leqslant h \leqslant 8$	$-8 \leqslant h \leqslant 9$
	$-4 \leqslant k \leqslant 4$	$-4 \leqslant k \leqslant 4$
	$-10 \leqslant l \leqslant 11$	$-10 \leqslant l \leqslant 10$
No. obs.refl. [a]	154	156
$R(\text{int})_{\text{obs}}$ [b]	1.46	1.11
Refinement		
R_{obs}	4.39	4.26
wR_{obs}	5.11	5.62
GoF$_{\text{obs}}$	3.96	4.42
No. pars.	38	38

[a]Criterion for the observed reflections is $|F_{\text{obs}}| > 3\sigma$.
[b]All agreement factors are given in %, weighing scheme is $1/[\sigma^2(F_{\text{obs}}) + (0.01F_{\text{obs}})^2]$.

symmetrically independent sites in the unit cell, which are now fully occupied by Li^{1+} (Table IV). Hence, the Li^{1+} cations are completely ordered above 11 GPa. The ordering of the Li^{1+} ions seems to correlate well with the pressure-induced increase of resistivity [8].

As the octahedral layers are basically identical in the low- and high-pressure polymorphs, it is plausible that there are no bonds broken within these layers during the phase transitions and in the intermediate phase. Stacking disorder can only occur if more than one energetically comparable position exists for the neighboring layer [23]. We postulate that during the phase transition above 9 GPa the octahedral layers are distributed between these two basically equivalent positions with stacking faults between them, giving rise to the one-dimensional diffuse scattering (Fig. 7). When the pressure is further increased, the polytypic intermediate phase is transformed to the polymorph without faults at about 11 GPa. The ordering of the Li^{1+} ions would influence the stacking disorder of the octahedral layers and could trigger the occurrence of the high-pressure nonpolytypic phase.

Many different polymorphs of $Li_xV_2O_5$ have been described in the literature and it is interesting to see whether the new high-pressure phase is similar to any of the known polymorphs in the vanadium bronze systems [24]. A comparison of the lattice parameters of the new high-pressure polymorphs obtained in this study with the reported lattice parameters by Galy [24] shows that they are clearly different, in particular, with respect to the monoclinic angle. We thus believe that the structure of the high-pressure phase of $Li_{0.33}V_2O_5$ above 11 GPa is a new polymorph in the already rich phase diagram of the vanadium bronzes. It remains to be seen whether

TABLE IV. Refined structural parameters in $\beta - Li_{0.33}V_2O_5$ at 11.08 and 12.87 GPa. The occupancies of the sites for all the atoms are all equal to 1.

	x	y	z	U_{iso}
11.08 GPa				
V1	− 0.3004(5)	0	0.1096(3)	0.010(5)
V2	− 0.0767(5)	0	0.1374(2)	0.010(5)
V3	− 0.3233(5)	0	0.4346(3)	0.006(5)
O1	0	0	0	0.009(2)
O2	− 0.798(2)	0	0.0490(12)	0.0059(16)
O3	− 0.607(2)	0	0.1012(13)	0.0067(15)
O4	− 0.3852(18)	0	0.2207(11)	0.0080(17)
O5	− 0.197(2)	0	0.2437(11)	0.0069(17)
O6	− 0.004(2)	0	0.2971(14)	0.0123(18)
O7	− 0.210(2)	0	0.5841(12)	0.0073(16)
O8	− 0.4087(19)	0	0.5304(11)	0.016(2)
Li	0	0	0.5	0.049(13)
12.87 GPa				
V1	− 0.3015(5)	0	0.1088(3)	0.006(5)
V2	− 0.0762(5)	0	0.1391(3)	0.006(5)
V3	− 0.3234(5)	0	0.4351(3)	0.013(5)
O1	0	0	0	0.011(2)
O2	− 0.799(2)	0	0.0482(13)	0.0079(16)
O3	− 0.6051(19)	0	0.1037(13)	0.0061(14)
O4	− 0.3872(19)	0	0.2199(12)	0.0093(16)
O5	− 0.199(2)	0	0.2449(13)	0.0090(16)
O6	− 0.004(2)	0	0.2988(15)	0.0139(18)
O7	− 0.209(2)	0	0.5837(13)	0.0087(16)
O8	− 0.4094(19)	0	0.5322(12)	0.016(2)
Li	0	0	0.5	0.048(12)

β-$Ag_{0.33}V_2O_5$ also follows the same transition path at higher pressures than the ones reached at this study. It is also interesting to clarify the anomalies of the lattice parameters and unit-cell volumes in β-$Na_{0.33}V_2O_5$ at about 12 GPa [20] on the basis of a detailed crystallographic study.

Yamauchi and Ueda [8] indicated that the nonsuperconducting phase of $Li_{0.33}V_2O_5$ above 10 GPa at room temperature could be the key to understand superconductivity in all the $A_{0.33}V_2O_5$ vanadium bronzes. In general, the electronic structure of β-$A_{0.33}V_2O_5$ can be regarded as weakly coupled two-leg ladder system formed by V2-V2 and V1-V3 ladders [25,26]. Presumably, the superconductivity is caused by the inter- and/or intraladder charge transfer or charge fluctuation induced by pressure [4]. In the ambient structure of $Li_{0.33}V_2O_5$, the V3 atoms form a ladder with the V1 atoms through the O5 atoms, with the angle V3-O5-V1 close to 180° (Fig. 1). The V3 atoms can interact with the V2 atoms through the O5 atoms. In the high-pressure structure, on the other hand, the V3 atoms are linked to the V1 atoms through the O4 atoms and the angle

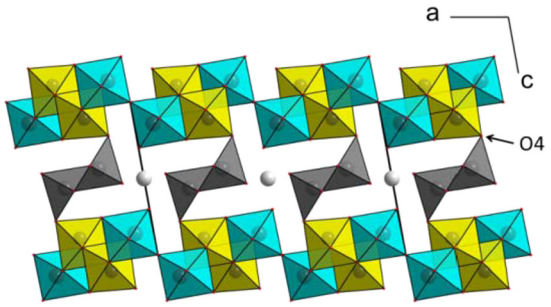

FIG. 8. (Color online) Crystal structure of $Li_{0.33}V_2O_5$ at 12.87 GPa (C2/m, $Z = 6$). The polyhedra around the V1, V2, and V3 atoms are drawn yellow, cyan, and dark gray, respectively. The gray symbols are the Li atoms. The O4 oxygen atom is indicated.

V3-O4-V1 is close to 90° (Fig. 8). This means that the V1-V3 ladder is broken and the system cannot be regarded as a coupled two-leg ladder system any longer. Furthermore, the V3 atoms are isolated from the V2 atoms as there is no link between the V3 and V2 atoms. Such a structure obstructs inter- and/or intraladder charge transfer or charge fluctuation, leading to a nonsuperconducting state. In our view, this loss of the two-leg ladder in the high-pressure phase of $Li_{0.33}V_2O_5$ could be the most significant reason for the absence of superconductivity.

Our observations thus strongly support the hypothesis that the underlying mechanism for superconductivity in the Wadsley-type $A_{0.33}V_2O_5$ vanadium bronzes is related to pressure-induced inter- and/or intraladder charge transfer or charge fluctuations in the two-leg ladder system present in the polymorphs with superconducting ground states [4,8].

The superconducting properties in the β-$A_{0.33}V_2O_5$ bronzes are sensitive to the content of the A cation so that the behavior of the A cations could be of some importance to the mechanisms of superconductivity [8]. The fact that the new high-pressure phase β-$Li_{0.33}V_2O_5$ determined in this study does not have a superconducting ground state might also be related to the fact that the distribution of the Li^{1+} ions between the layers is entirely ordered.

IV. CONCLUSIONS

β-$Li_{0.33}V_2O_5$ undergoes a sequence of pressure-induced phase transitions at 9 and 11 GPa associated with the stacking disorder of the octahedral layers and the collapse of tunnels at which the Li^{1+} cations are located. The distribution of the Li^{1+} cations in the vanadate framework is fully ordered in the polymorph above 11 GPa. No pressure-induced increase of the coordination numbers of vanadium is observed. There is also no evidence for the charge ordering of mixed-valence vanadium. The loss of the two-leg ladder V1-V3 in the high-pressure phase could be the most significant reason for the absence of superconductivity.

[1] A.D. Wadsley, Acta Crystallogr. **8**, 695 (1955).
[2] I. Yamauchi, M. Itoh, T. Yamauchi, J.-I. Yamaura, and Y. Ueda, J. Phys.: Conf. Series **200**, 012234 (2010).
[3] J.-I. Yamaura, M. Isobe, H. Yamada, T. Yamauchi, and Y. Ueda, J. Phys. Chem. Solids **63**, 957 (2002).
[4] K. Ohwada, T. Yamauchi, Y. Fujii, and Y. Ueda, Phys. Rev. B **85**, 134102 (2012).

[5] T. Yamauchi, Y. Ueda, and N. Môri, Phys. Rev. Lett. **89**, 057002 (2002).
[6] T. Yamauchi, H. Ueda, and Y. Ueda, Physica C **460–462**, 66 (2007).
[7] T. Kozuka, M. Itoh, N. Takeshita, C. Terakura, T. Yamauchi, Y. Ueda, H. Takagi, and Y. Tokura, J. Magn. Magn. Mater. **310**, 1110 (2007).
[8] T. Yamauchi and Y. Ueda, Phys. Rev. B **77**, 104529 (2008).
[9] T. Suzuki, I. Yamauchi, Y. Shimizu, M. Itoh, N. Takeshita, C. Terakura, H. Takagi, Y. Tokura, T. Yamauchi, and Y. Ueda, Phys. Rev. B **79**, 081101(R) (2009).
[10] H. K. Mao, J. Xu, and P. M. Bell, J. Geophys. Res. **91**, 4673 (1986).
[11] H. Ahsbahs, Z. Kristallogr. **219**, 305 (2004).
[12] X-Area: Stoe IPDS Software, Stoe & Cie GmbH, Darmstadt, Germany.
[13] M. Merlini and M. Hanfland, High Pressure Research **33**, 511 (2013).
[14] Crysalis software system, Oxford Diffraction Ltd, Abingdon, England.
[15] A. Altomare, M. C. Burla, M. Camalli, G. L. Cascarano, C. Giacovazzo, A. Gugliardi, A. G. G. Moliterni, G. Polidori, and R. Spagna, J. Appl. Crystallogr. **32**, 115 (1999).
[16] V. Petříček, M. Dušek, and L. Palatinus, Z. Kristallogr. **229**, 345 (2014).
[17] K. Friese, Y. Kanke, and A. Grzechnik, Acta Crystallogr. B **65**, 326 (2009).
[18] J. M. Posse, K. Friese, and A. Grzechnik, J. Phys.: Condens. Matter **23**, 215401 (2011).
[19] K. Friese, A. Grzechnik, J. M. Posse, and V. Petricek, High Pres. Res. **33**, 196 (2013).
[20] K. Rabia, A. Pashkin, S. Frank, G. Obermeier, S. Horn, M. Hanfland, and C. A. Kuntscher, High Press. Res. **29**, 504 (2009).
[21] A. Grzechnik, Chem. Mater. **10**, 2505 (1998).
[22] A. Grzechnik, T.-Z. Ren, J. M. Posse, and K. Friese, Dalton Trans. **40**, 4572 (2011).
[23] H. Katzke, Z. Kristallogr. **216**, 278 (2001).
[24] J. Galy, J. Solid State Chem. **100**, 229 (1992).
[25] M.-L. Doublet and M.-B. Lepetit, Phys. Rev. B **71**, 075119 (2005).
[26] T. Suzuki, I. Yamauchi, M. Itoh, T. Yamauchi, and Y. Ueda, Phys. Rev. B **73**, 224421 (2006).